Noname manuscript No.
(will be inserted by the editor)

The effect of depletion of radicals on freely propagating hydrocarbon flames

Vladimir V. Gubernov · Sergei S. Minaev · Valeri I. Babushok · Andrey V. Kolobov

Received: date / Accepted: date

Abstract In this work we investigate the properties and stability of deflagration waves in the model which include the two-step chain-branching reaction mechanism, first order reaction of conversion of radicals into products, and Newtonian cooling to the surroundings. The propagation velocity, the maximum temperature and concentration of radicals monotonically decay as the rate of the radical termination reaction is increased. The critical parameter values for the onset of instabilities and quenching of the travelling combustion wave are found. It is demonstrated that the depletion of radicals through the additional termination reaction enhances the onset of instabilities and extinction. The comparison of the efficiency of the radical and thermal quenching mechanisms is performed. The solutions emerging once the travelling deflagration wave becomes unstable are studied.

Keywords premixed flames · thermal-diffusive instabilities · flammability limit · radical depletion

1 Introduction

Propagation of deflagration waves in hydrocarbon fuel mixtures is usually described by the models with chain-branching reaction mechanism [1]. It is known

V. V. Gubernov
P.N. Lebedev Physical Institute of Russian Academy of Sciences, Moscow, Russia E-mail: gubernov@lpi.ru
Far Eastern Federal University, Vladivostok, Primorsky Krai, Russia

S. S. Minaev
Far Eastern Federal University, Vladivostok, Primorsky Krai, Russia

V. I. Babushok
Far Eastern Federal University, Vladivostok, Primorsky Krai, Russia

A. V. Kolobov
P.N. Lebedev Physical Institute of Russian Academy of Sciences, Moscow, Russia

that such processes as Soret diffusion [2–8], radical-wall interaction [9–17], adding of flame inhibitors/flame suppressants [18,19] can affect the concentration of radicals in the reaction zone and thus influence the flame speed, structure and stability and modify the flammability limits.

In hydrocarbon flames the inclusion of Soret diffusion affects the mass fluxes of light components of reacting mixtures, mainly, H and H_2 [2–7]. In freely propagating flames it is sufficient to consider the thermal diffusion of H radicals, which causes the additional flux of H atoms in the downstream direction. This reduces the concentration of H radicals in the reaction zone and thus modifies the rates of the reactions involving hydrogen atoms. As a result the mass flow velocity of the deflagration calculated with and without Soret diffusion is lower in the first case for both lean and rich mixtures. In the case of stretched flames the thermal diffusion of H_2 becomes important. It is shown that the flammability limits are significantly influenced by the Soret effect in this case [2,3,8].

The gas-solid wall interaction is the other route for the reduction of the concentration of radicals in addition to the transport mechanisms discussed above. This is especially important in micro-flow configurations, where the role of the surface effects is enhanced due to the increase of surface-to-volume ratio [13,15]. To some extent the radical quenching on the walls can be treated as an additional reaction of the radical species decay [9,10]. More detailed consideration reveals that several processes should be taken into consideration including the adsorption of radicals on the walls, heterogeneous recombination reaction and desorption of products. The latter two stages usually also release heat, which is added to the overall energy balance [11]. In most cases the rate limiting step is the radical adsorption and the recombination kinetics is much faster. Thus it is important to consider two processes: radical quenching and heat release [11]. Numerical modelling reveals that radical termination mechanism can affect the properties of the flames, and shift the limits of ignition and extinction in the case of radical species interaction with hot walls [11–14]. The main source of uncertainty in such analysis is the sticking coefficient, which takes the values from 0 to 1. It depends on the material of the solid wall and in some models is deliberately overestimated in order to understand the maximum extent of the role of radical quenching [11,12]. Recent experimental observations show that the sticking coefficients for typical surface of micro-flow reactors are relatively small and it was found that the radical interaction with the surface has some influence on the combustion characteristics in the case of hot walls and decreased pressures [15–17].

Besides the interfacial mechanisms the homogeneous reactions can also influence the concentration of radical species in flame reaction zone. In [18,19] the Zeldovich–Linan [20,21] model with chain-branching reaction kinetics is used to analyse the freely propagating combustion waves and additional processes were included to describe influence/effect of chemical inhibitors. Additional processes were the endothermic stage of inhibitor decomposition producing the radical scavenger species and subsequent termination reaction of scavenger with radicals. Suggested mechanism was used to model the decrease of burning velocity as a result of inhibitor addition.

It is interesting to note that there are several reasons of current interest to flame inhibition studies. The use of flame inhibitors allows one to control different parameters of combustion, such as reaction rate, burning or detonation velocity, explosion limits, flame thickness, ignition delay etc. On the other hand effective

flame inhibitors are used as fire suppressant agents. Recent practical interest is in finding of suitable replacement for halon 1301 [22] due to its high ozone depletion potential (ODP). Detailed kinetic modelling studies of flame inhibition processes were conducted in [23–25]. Development of simplified and global kinetic models of flame inhibition should allow theoretical studies of more complicated physical models and application of CFD models for complex geometries and complex hydrodynamic flows with combustion.

The aim of this work is the further studies of simple kinetic model of chain-branching combustion reaction with typical linear radical termination steps imitating inhibition processes. We used the two stage Zeldovich–Barenblatt model [26] to describe the chain-branching mechanism of deflagration propagation, while the first order radical termination reaction is employed to introduce the radical depletion mechanism. This approach follows the analysis of the effect of radical-wall interaction on flames in [9, 10, 14]. However here we do not restrict the consideration to the interfacial effects only and consider the generic radical sink mechanism which can represent different phys-chemical processes related to reduction of radical species in the reaction zone. The paper is focused on the investigation of critical phenomenon in deflagrations, namely, extinction and the onset of instabilities, which has not been analysed previously in this type of models.

2 Model

We consider a generalized model for premixed flame propagating that includes two steps: auto-catalytic chain branching $\mathrm{A} + \mathrm{R} \to 2\mathrm{R}$ and recombination $\mathrm{R} + \mathrm{M} \to \mathrm{P} + \mathrm{M}$. Here A is the fuel, R are radicals, P is the product, and M is a third body. It is assumed that all the heat of the reaction is released during the recombination stage and the chain branching stage does not produce or consume any heat. This model was introduced in [26] and considered in many aspects later [27–31]. Here it is complemented with the additional reaction step $\mathrm{R} \to \mathrm{P}$ representing the generalized radical sink. The approach is similar to analysis in [9, 10, 14]. The thermal effect of this reaction is taken to be negligible in comparison with the heat release rate of the main recombination reaction.

Governing equations for this process can be written as

$$\begin{aligned}
\rho c_p \frac{\partial T}{\partial t} &= \lambda \Delta T + \rho Q A_r Y_R - \alpha \frac{S}{V}(T - T_0), \\
\rho \frac{\partial Y_A}{\partial t} &= \rho D_A \Delta Y_A - W_A A_b \frac{\rho Y_A}{W_A} \frac{\rho Y_R}{W_R} e^{-E/RT}, \\
\rho \frac{\partial Y_R}{\partial t} &= \rho D_R \Delta Y_R + W_R \left(A_b \frac{\rho Y_A}{W_A} \frac{\rho Y_R}{W_R} e^{-E/RT} - A_r \frac{\rho Y_R}{W_R} \frac{\rho}{M} - K \frac{\rho Y_R}{W_R} \right),
\end{aligned} \tag{1}$$

where T is the temperature; Y_A and Y_R represent the mass fractions of fuel and radicals respectively; ρ is the density; c_p is the specific heat; W_A, W_R, and M are the fuel, radical, and mean molecular weights, respectively; D_A and D_R represent the diffusivities of fuel and radicals respectively, A_r and A_b are constants of recombination and chain branching reactions respectively; Q is the heat of the recombination reaction; E is the activation energy for chain branching reaction; R

is the universal gas constant; α is the heat exchange coefficient from the volume V of the gaseous fuel confined by the surface S to the surroundings kept at the temperature T_0; K is the coefficients of radical quenching.

The radical quenching mechanism can be of various nature. It can be caused by the volumetric inhibition reaction of the type $\mathrm{R} + \mathrm{In} \to \mathrm{P}_1$, where the inhibitor concentration X_{In} is much higher than the radical concentration X_R and the consumption of In species is neglected. In this case K is the rate of the inhibition reaction. Also the mechanism of radical quenching on the walls can be considered with the rate of adsorption of radicals given as $h_m X_R$, where h_m can be found from the Langmuir adsorption isotherm [32]. In this case $K = h_m \dfrac{S}{V}$.

We define the non dimensional variables

$$t' = \Omega t,\ \ x' = \sqrt{\frac{\Omega}{\kappa}} x,\ \ \theta = \frac{T}{T_b},\ \ y_{_A} = \frac{Y_A}{Y_A^{-\infty}},\ \ y_{_R} = \frac{Y_R W_A}{Y_A^{-\infty} W_R}, \tag{2}$$

where $\Omega = \dfrac{\rho A_r}{W}$ is characteristic frequency associated with the rate of recombination reaction; $\kappa = \dfrac{\lambda}{\rho c_p}$ is thermal diffusivity; $T_b = T_0 + \dfrac{QWY_A^{-\infty}}{c_p W_A}$ is the adiabatic combustion temperature; $Y_A^{-\infty}$ is the mass fraction of fuel in fresh unreacted mixture, which is positive number; $\beta = \dfrac{E}{RT_b}$ is the activation energy of the branching reaction.

Introducing the non dimensional parameters

$$r = \frac{A_b W Y_A^{-\infty}}{A_r W_A e^{\beta}},\ L_{A,R} = \frac{\rho c_p D_{A,R}}{\lambda},\ h = \frac{\alpha}{\rho c_p \Omega}\frac{S}{V},\ k = \frac{K}{\Omega}. \tag{3}$$

the governing equations for the non dimensional temperature, θ, concentration of fuel, y_A, and radicals, Y_R, can be written in non dimensional form as

$$\begin{aligned}
\frac{\partial \theta}{\partial t} &= \Delta\theta + (1-\theta_0) y_{_R} - h(\theta - \theta_0),\\
\frac{\partial y_{_A}}{\partial t} &= L_A^{-1} \Delta y_{_A} - r y_{_A} y_{_R} e^{\beta(1-1/\theta)},\\
\frac{\partial y_{_R}}{\partial t} &= L_R^{-1} \Delta y_{_R} + r y_{_A} y_{_R} e^{\beta(1-1/\theta)} - (1+k) y_{_R},
\end{aligned} \tag{4}$$

where primes are omitted, L_A and L_R are the Lewis numbers for fuel and radicals respectively; β is the dimensionless activation energy of the chain-branching step; r is the ratio of the characteristic times of the recombination and branching steps; h is the heat loss coefficient, $\theta_0 = T_0/T_b$ is the ambient temperature; k is the radical quenching coefficient. In the case of radical quenching on the walls the coefficients h and k can be expressed in terms of dimensionless parameters as $h = Nu/d^2$ and $k = Sh/L_R d^2$, where Nu and Sh are Nusselt and Sherwood numbers, respectively, while d is the dimensionless ratio of V and S.

3 Results

3.1 Travelling waves

In order to investigate the properties and the structure of the deflagration waves we introduce the flame coordinate as $\xi = x - ct$, where u represents the flame speed. This allows to reduce the governing partial differential equations (4) to the system of ordinary differential equations

$$\begin{aligned} &\theta_{\xi\xi} + u\theta_\xi + (1-\theta_0)y_R - h(\theta-\theta_0) = 0, \\ &L_A^{-1} y_{A\xi\xi} + u y_{A\xi} - r y_A y_R e^{\beta(1-1/\theta)} = 0, \\ &L_R^{-1} y_{R\xi\xi} + u y_{R\xi} + r y_A y_R e^{\beta(1-1/\theta)} - (1+k) y_R = 0, \end{aligned} \tag{5}$$

The boundary conditions are defined as

$$\begin{aligned} &\theta = \theta_0,\ y_A = 1, \quad y_R = 0 \ \text{ for } \ \xi \to \infty, \\ &\theta_\xi = 0,\ y_{A\xi} = 0,\ y_R = 0 \ \text{ for } \ \xi \to -\infty, \end{aligned} \tag{6}$$

which correspond to the combustion wave propagating in the positive x direction. On the right boundary (fresh mixture) we have cold and unburned state, where the fuel has not been consumed yet and no radicals have been produced. On the left boundary ($\xi \to -\infty$) we require that there is no reaction occurring so the solution reaches a steady state of (5). Therefore the derivatives of θ, y_A are set to zero and $y_R = 0$ for $\xi \to -\infty$. The downstream temperature reaches a constant value, which is equal to the adiabatic flame temperature or the ambient temperature in the adiabatic ($h = 0$) or non-adiabatic ($h > 0$) case, respectively.

The equations (5) subject to the boundary conditions (6) constitute the boundary value problem, which is solved numerically using a standard shooting algorithm with a fourth–order Runge–Kutta integration scheme first and then the results are corrected by employing the relaxation algorithm with Newton method. The results of the numerical integration are presented in Figs. 1 and 2. The solution profiles, $\theta(\xi)$ and $y_R(\xi)$, are plotted in Fig. 1 for $L_A = 10$, $L_R = 1$, $\beta = 8.0$, $r = 10^3$, $h = 10^{-2}$, $\theta_0 = 0.15$ and three different values of k. It should be noted that the integration domain for numerical algorithm is several times larger than it is shown in Fig. 1, where the coordinate is scaled as shown in the figure caption. The inclusion of the radical sink reaction path clearly affects the distribution of temperature and species in the deflagration wave. The intensification of the recombination of radicals with the increase of k results in the reduction of peak values of y_R. Since the heat release rate is proportional to y_R this also causes the decrease of the maximum temperature in the combustion wave. It is interesting to note that the dependence of peak values of radical mass fraction and temperature, $\max_\xi\{y_R\}$ and $\max_\xi\{\theta\}$, on k is close to linear function for $k \in [0, 0.1]$.

In Fig. 2 the dependence of the flame speed u on the dimensionless activation energy of the branching reaction, β, is plotted for $L_A = 10$, $L_R = 1$, $r = 10^3$, $h = 10^{-2}$, $\theta_0 = 0.15$ and various values of k in the range from 0 to 0.5. For fixed parameter values $u(\beta)$ is characterized by a turning point (β_{tp}, C_{tp}), corresponding to the extinction of the travelling combustion waves. The turning point type of

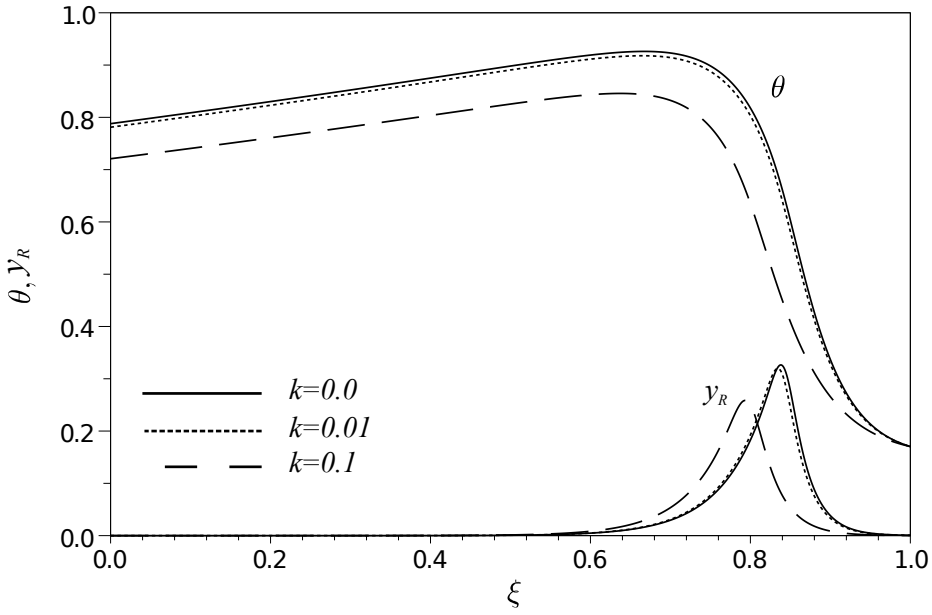

Fig. 1 Distribution of temperature, $\theta(\xi)$, and radicals, $y_R(\xi)$, in the deflagration wave for $L_A = 10$, $L_R = 1$, $\beta = 8.0$, $r = 10^3$, $h = 10^{-2}$, $\theta_0 = 0.15$ and $k = 0$ (solid line), $k = 10^{-2}$ (dotted line), $k = 10^{-1}$ (dashed line). The coordinate is scaled over 55.1, 54.5, and 49.4 for $k = 0$, 10^{-2}, and 10^{-1}, respectively.

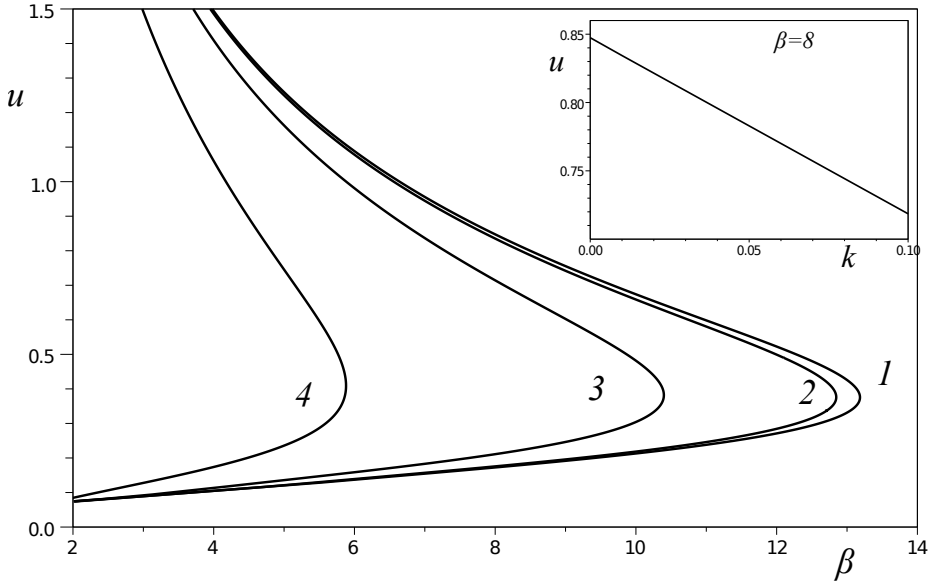

Fig. 2 Flame speed, u, as function of β for $L_A = 10$, $L_R = 1$, $r = 10^3$, $h = 10^{-2}$, $\theta_0 = 0.15$ and $k = 0$ (curve '1'), $k = 10^{-2}$ (curve '2'), $k = 10^{-1}$ (curve '3'), and $k = 0.5$ (curve '4').

critical behaviour is also called fold bifurcation. If the activation energy is less than the critical value for the extinction, β_{tp}, then there exist two solution branches propagating with different velocities. For $\beta > \beta_{tp}$ travelling wave solutions do not exist. As it is discussed below the lower solution branch is completely unstable and cannot be realized in experiments. Therefore we focus on the upper (fast) branch only. In particular the solution profiles in Fig. 1 correspond to the fast solution branch. It is seen that the increase of k shifts the critical value of the activation energy for the turning point, β_{tp}, towards smaller values from $\beta_{tp} \approx 13.2$ for $k = 0$ to $\beta_{tp} \approx 5.88$ for $k = 0.5$. In the inset to the Fig. 2 the dependence of u on k is illustrated for fixed value of $\beta = 8.0$. The function $u(k)$ demonstrates the linear behaviour.

This can be shown exactly, if we consider equations (5) for the vector function $\mathbf{u} = [\theta,\ y_A,\ y_R]^T$ in the form

$$\left(\hat{\mathbf{D}} d^2/d\xi^2 + u d/d\xi \hat{\mathbf{I}}\right) \mathbf{u} + \hat{\mathbf{N}}(\mathbf{u}) = \mathbf{0} \tag{7}$$

where we have introduced $\hat{\mathbf{I}}$ - a 3×3 identity matrix,

$$\hat{\mathbf{D}} = \begin{bmatrix} 1 & 0 & 0 \\ 0 & L_A^{-1} & 0 \\ 0 & 0 & L_R^{-1} \end{bmatrix}, \tag{8}$$

the reaction terms are defined as

$$\hat{\mathbf{N}}(\mathbf{u}) = \begin{bmatrix} (1-\theta_0) y_R - h(\theta - \theta_0) \\ -r y_A y_R e^{\beta(1-1/\theta)} \\ r y_A y_R e^{\beta(1-1/\theta)} - (1+k) y_R \end{bmatrix}. \tag{9}$$

Now let $\mathbf{u_0}(\xi)$ be a travelling wave solution of (7) for $k = 0$ and let us differentiate (7) with respect to k to give

$$\hat{\mathbf{L}}\mathbf{w} = -\frac{\partial u}{\partial k}\frac{\partial \mathbf{u}_0}{\partial \xi} - \frac{\partial \hat{\mathbf{N}}}{\partial k}, \tag{10}$$

where $\hat{\mathbf{L}} = \hat{\mathbf{D}}\partial^2/\partial\xi^2 + u\partial/\partial\xi\hat{\mathbf{I}} + \hat{\mathbf{M}}(\xi)$ is the linear differential operator, $\hat{\mathbf{M}}(\xi) = \partial\hat{\mathbf{N}}/\partial\mathbf{u}$ is the Jacobi matrix evaluated at $\mathbf{u}_0(\xi)$ and $\mathbf{w} = \partial\mathbf{u}_0/\partial k$. Together with the problem (7–9) an adjoint problem $\hat{\mathbf{L}}^+\mathbf{z}(\xi) = \lambda\mathbf{z}(\xi)$ is considered, where $\hat{\mathbf{L}}^+ = \hat{\mathbf{D}}\partial^2/\partial\xi^2 - u\partial/\partial\xi\hat{\mathbf{I}} + \hat{\mathbf{M}}(\xi)^T$. The adjoint problem also has bounded solutions $\mathbf{z}^{(0)}$ corresponding to $\lambda = 0$. For the existence of the solutions of the problem (10) the right hand side should be orthogonal to the solution of the homogeneous adjoint problem i.e. the following condition for the solution existence has to be satisfied

$$\frac{\partial u}{\partial k} = \frac{\langle \mathbf{z}^{(0)}, \partial\mathbf{N}/\partial k\rangle}{\langle \mathbf{z}^{(0)}, \partial\mathbf{u}_0/\partial\xi\rangle}. \tag{11}$$

The standard inner product is used in (11) i.e. $\langle \mathbf{f}, \mathbf{g}\rangle = \int_{-\infty}^{+\infty} d\xi \mathbf{f}(\xi)\mathbf{g}(\xi)$ and to evaluate integral the solutions $\mathbf{z}^{(0)}$ and $\mathbf{u}_0$ the corresponding equations has to solved numerically as it is done in [33]. The relation (11) indicates that for small values of k there is a linear dependence of the flame speed on the rate of the radical scavenging reaction as demonstrated in the inset to Fig. 2.

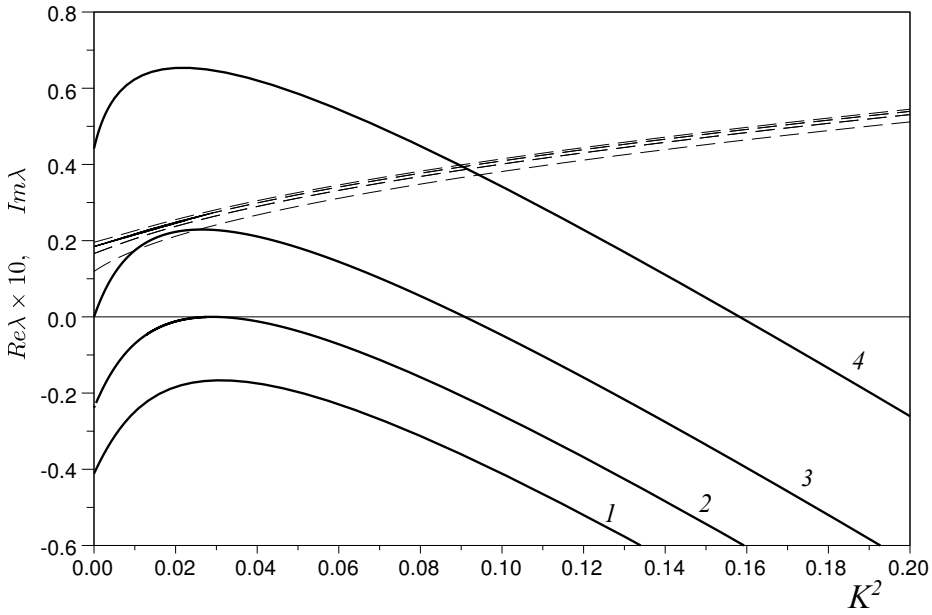

Fig. 3 The dispersion relations $\mathrm{Re}\lambda(K^2)$ and $\mathrm{Im}\lambda(K^2)$ shown with the solid and the dashed lines, respectively, for $L_A = 10$, $L_R = 1$, $r = 10^3$, $h = k = 0.01$, $\theta_0 = 0.15$, $\beta = 11.7$ (curve '1'), 12 (curve '2'), 12.15 (curve '3'), and 12.32 (curve '4').

3.2 Linear stability of deflagration

To analyse the stability of the travelling combustion waves the governing equations (4) are linearised near the travelling wave solution in order to obtain the linear stability problem which describes the evolution of the infinitely small perturbations of the travelling wave. We seek the solution of the form $\mathbf{u}(\xi,t) = \mathbf{u}(\xi) + \epsilon\mathbf{v}(\xi)\exp(\lambda t + iKy)$, where $\mathbf{u}(\xi)$ represents the travelling combustion wave, terms proportional to the small parameter ϵ are the linear perturbation terms, λ is the increment of exponential growth of perturbation, K is the wave number of the perturbation in the direction, orthogonal to the propagation direction along x axis. Substituting this expansion into (4), leaving terms proportional to the first order of ϵ only we obtain

$$\hat{\mathbf{L}}\mathbf{v} = \lambda\mathbf{v} + K^2\hat{\mathbf{D}}\mathbf{v}. \tag{12}$$

The eigenvalue problem (12) is complemented with the boundary conditions $|\mathbf{v}| \to 0$ as $\xi \to \pm\infty$. Here it is solved numerically by finding the dispersion relations $\lambda(K)$ of $\hat{\mathbf{L}}$ in a complex plane using the Evans function method implemented with the use of a compound matrix approach as discussed in [29]. We skip here the details of the technique and proceed to the description of the new results.

It is found that two types of instabilities may occur in the system depending on the Lewis number for fuel L_A. For $L_A > 1$ the travelling instabilities emerge which are characterized by complex dispersion relations illustrated in Fig. 3 for $L_A = 10$, $L_R = 1$, $r = 10^3$, $h = k = 0.01$, $\theta_0 = 0.15$, and different values of β. The real and imaginary parts of $\lambda(K)$ are plotted with the solid and dashed lines, respectively. The imaginary branches $Im\lambda(K)$ are located very close to each other

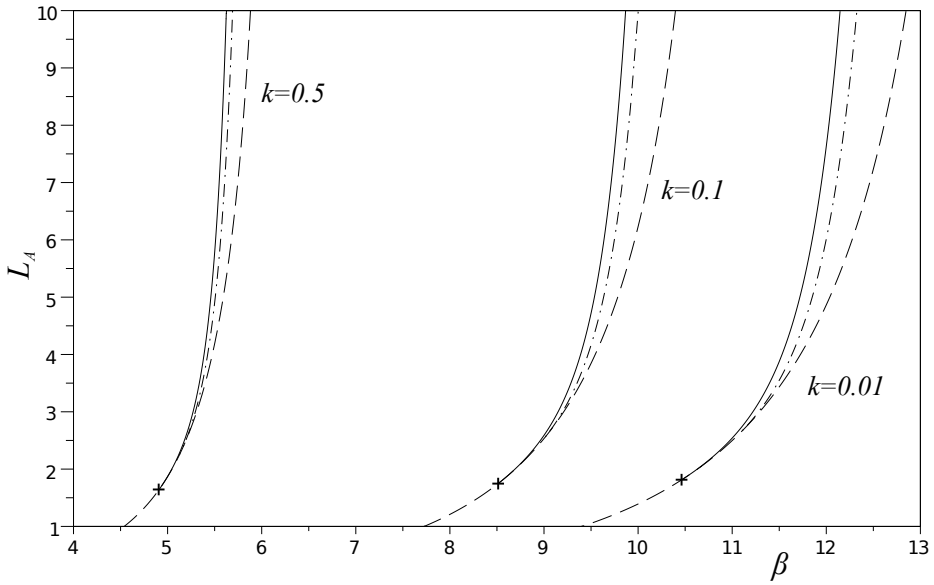

Fig. 4 Critical parameter values for the onset of travelling instabilities (solid line), Hopf (dashed dotted line) and fold (dashed line) bifurcations in the L_A vs β plane for $L_R = 1$, $r = 10^3$, $h = 10^{-2}$, $\theta_0 = 0.15$ and $k = 0.5$, 0.1 and 0.01. The points where the solid and dashed lines merge are shown with '+' symbols.

for various β considered here. It should be noted here that the dispersion relations of the problem (12) are always symmetric with respect to real axis since $\hat{\mathbf{L}}$ is linear differential operator with real coefficients. Thus the complex conjugate part of $\lambda(K)$ is not shown in Fig. 3. The dispersion relation for stable combustion wave with $Re\lambda < 0$ for all K is illustrated with curve '1' for $\beta = 11.7$. As β is increased to 12 the maximum of the real part of the dispersion relation approaches the real axis at the finite K_m i.e. $Re\lambda(K_m) = 0$ in such a way that $Im\lambda(K_m) \neq 0$. Thus the travelling instabilities of the deflagration wave emerge for this specific value of $\beta_{tr} \approx 12$. For larger values of β the real part of the dispersion relation grows for all wave numbers, K. At the second critical value $\beta_h \approx 12.15$ the value of $Re\lambda(0)$ changes sign from negative to positive, while $Im\lambda(0) \neq 0$. This is the Hopf bifurcation point, when the travelling wave solution losses stability in the one-dimensional case. For $\beta > \beta_h$ the deflagration wave is unstable with respect to the perturbations with $K \geq 0$ in certain interval of values, where $Re\lambda > 0$, as it is shown by the curve '4' in Fig. 3.

The results of the bifurcation analysis for the case $L_A > 1$ are summarized in Fig. 4, where the critical parameter values for the emergence of travelling instabilities, Hopf and fold bifurcation are plotted in the L_A vs β plane with the solid, dash-dotted and dashed lines, respectively. The other parameter values are chosen as $L_R = 1$, $r = 10^3$, $h = 10^{-2}$ and $k = 0.01$, 0.1 and 0.5. It is seen that for fixed value of k the stability of deflagration is lost via the multidimensional travelling instability prior to the onset of one-dimensional pulsating instabilities. There is a specific point shown with the '+' symbol, where all the critical curves intersect, which is a Bogdanov–Takens bifurcation point similar to the one re-

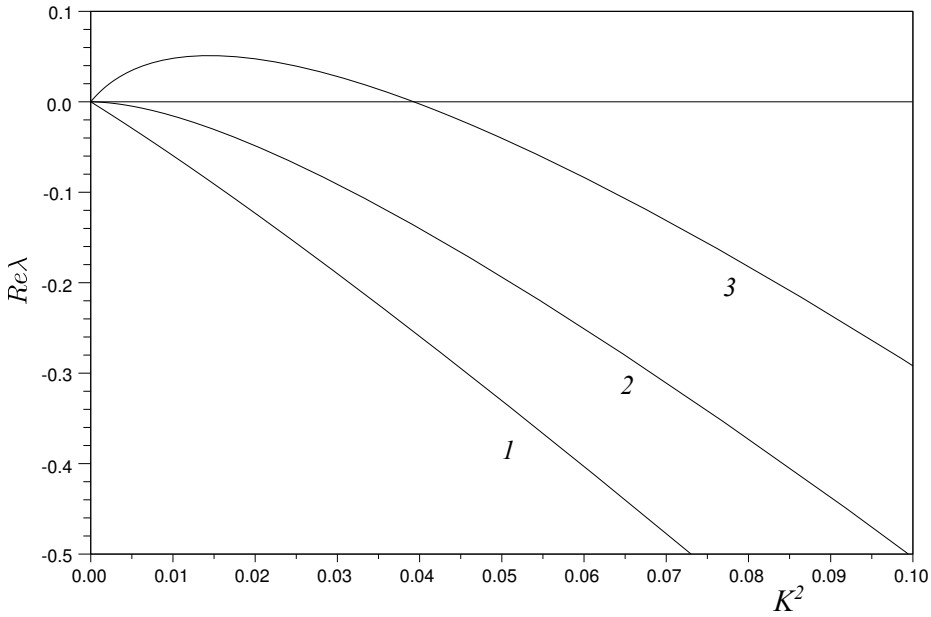

Fig. 5 The dispersion relations $Re\lambda(K^2)$ for $L_R = 1$, $r = 10^3$, $h = k = 0.01$, $\theta_0 = 0.15$, $\beta = 8$, $L_A = 0.9$ (curve '1'), 0.81 (curve '2'), and 0.7 (curve '3').

ported in [29]. It can be characterized by the critical value of the Lewis number for fuel $L_A^{BT} > 1$ and as L_A tends to L_A^{BT} from the above K_m and $Im\lambda(K_m)$ vanish. For $1 < L_A < L_A^{BT}$ the fast solution branch becomes completely stable up to the turning point, whereas the slow solution branch remain unstable. For this reason the neutral stability boundary and the Hopf bifurcation loci shown with the solid and dash-dotted line in Fig. 4 are discontinued for $L_A < L_A^{BT}$ and the dashed line corresponding to the fold bifurcation is only plotted for this case. In overall, as parameter k is increased and the radicals are becoming more depleted in the reaction zone the deflagration wave is getting more unstable. All the critical curves are uniformly shifted towards smaller value of the activation energy, β.

For the case of $L_A < 1$ the cellular instabilities emerge which are characterized by the purely real ($Im\lambda = 0$) dispersion relation shown in Fig. 5 for $L_R = 1$, $r = 10^3$, $h = k = 0.01$, $\theta_0 = 0.15$, $\beta = 8$, and different values of $L_A = 0.7$, 0.81, and 0.9. If the Lewis number for fuel is close to one the deflagration is stable and the real part of the dispersion relation is negative for all wave numbers except $K = 0$ for which $\lambda = 0$. The typical dispersion relation for this case is illustrated in Fig. 5 with curve '1' for $L_A = 0.9$. As L_A is decreased to the critical value 0.81... for the onset of cellular instabilities shown with curve '2' in Fig. 5 the function $\lambda(K)$ becomes tangent to the K-axis at the origin. Further modification of L_A below the critical value changes the dispersion relation so that there emerges a range of wave numbers K starting from zero to certain $K_c > 0$, for which $Re\lambda > 0$. This is demonstrated in Fig. 5 with the curve '3' for $L_A = 0.7$, where it is seen that the real part of the dispersion relation is positive for $K^2 \in [0, K_c^2]$ and $K^2 \approx 0.04$. In this way the cellular instabilities are established in the system. It is worthwhile noting that for this type of the instability onset the critical wave number grows

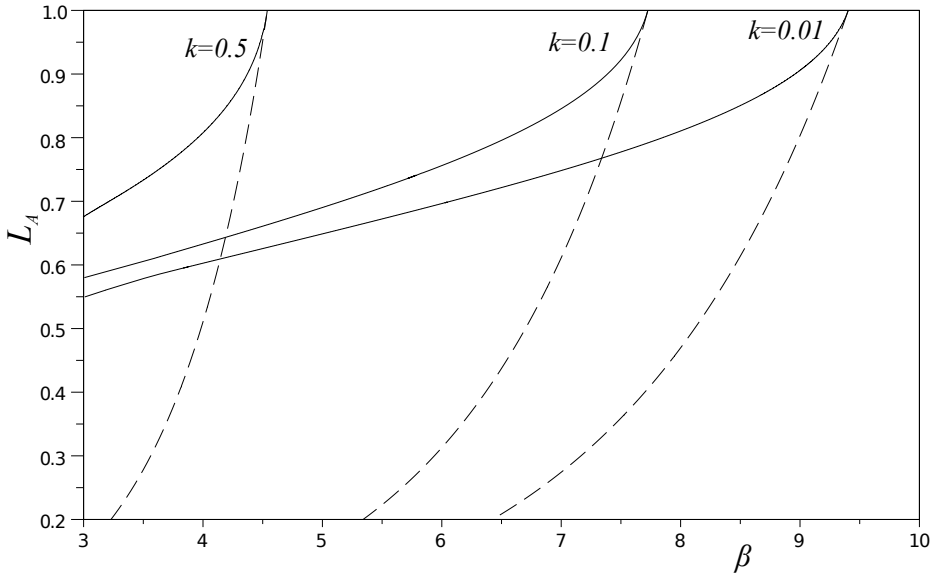

Fig. 6 Critical parameter values for the onset of cellular instabilities (solid line) and Fold bifurcation (dashed line) in the L_A vs β plane for $L_R = 1$, $r = 10^3$, $h = 10^{-2}$, $\theta_0 = 0.15$ and $k = 0.5$, 0.1 and 0.01.

from $K_c = 0$ at the critical point to larger positive values as the bifurcation parameter is further changed away from the neutral stability boundary into the unstable region of parameters. Therefore, there is certain difficulty in determining the critical parameter values for the emergence of cellular instabilities by direct integration of the governing partial differential equations (4), since in this case a very large domain of integration in the direction transverse to the propagation direction should be taken. Thus the spectral algorithms like the Evans function method are more convenient to solve this type of problems.

The results of the stability analysis for the case $L_A < 1$ are summarized in Fig. 6, where the critical parameter values, L_A vs β, for the onset of the cellular instabilities and the fold bifurcation are plotted with the solid and the dashed lines, respectively. The results are presented for $L_R = 1$, $r = 10^3$, $h = 10^{-2}$ and different values of $k = 0.01$, 0.1, and 0.5. For fixed value of k the critical curves merge as $L_A \to 1$, while as L_A is decreased from 1 the neutral stability boundary and the fold loci diverge so that for both curves the critical values of β monotonically decrease as L_A is becoming smaller. The influence of the radical sink reaction rate k can be seen in Fig. 6 as the shift of all critical loci to smaller values of β with the increase of k.

3.3 Radical vs thermal quenching

In order to estimate the effect of different factors i.e. radical depletion in the reaction zone and heat loss to the surroundings, we plot the dependence of the critical values of activation energy, β_c, for the onset of travelling, cellular instabilities and fold bifurcation as functions of either k or h.

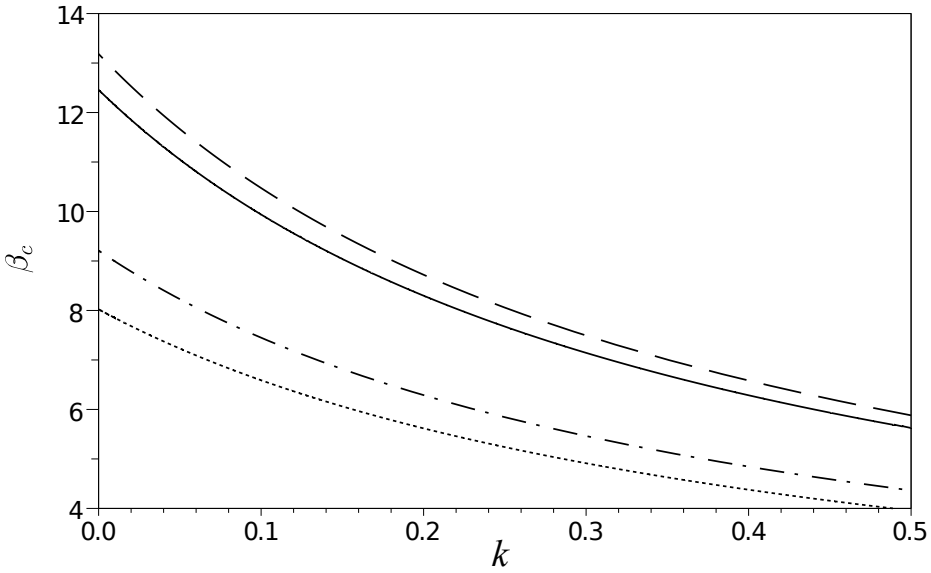

Fig. 7 The dependence of critical values of β on k for $L_R = 1$, $r = 10^3$, $h = 0.01$, $\theta_0 = 0.15$ and different values of L_A: (i) the travelling instability and fold bifurcation loci are shown with the solid and the dashed lines, respectively, for $L_A = 10$; (ii) the cellular instability and the fold bifurcation loci are plotted with the dotted and the dash-dotted lines, respectively, for $L_A = 0.8$.

In Fig. 7 the dependence of β_c on k is shown for $L_R = 1$, $r = 10^3$, $h = 0.01$, $\theta_0 = 0.15$. The travelling instability and fold bifurcation loci are shown with the solid and the dashed lines, respectively, for $L_A = 10$, whereas the cellular instability and the fold bifurcation loci are plotted with the dotted and the dash-dotted lines, respectively, for $L_A = 0.8$. All critical curves show monotonically decreasing behaviour as k is increased. In the case of $L_A = 10$ the neutral stability boundary (solid curve) related to the emergence of travelling instabilities is located below the fold bifurcation curve (dashed line) with difference in β_c of about 5% for all k values considered here. For $L_A = 0.8$ the graph of $\beta_c(k)$ for the emergence of cellular instabilities (dotted line) is located below the fold bifurcation curve (dash-dotted line) so that the critical values of β differ by $10-15\%$. In general, all critical curves $\beta_c(k)$ have finite derivative with respect to k at the origin and they can be estimated by the order in magnitude as $d(\ln \beta_c)/dk \sim O(1)$. Thus in order to obtain the 1% variation in β_c for any of the critical conditions the rate of radical depletion should be of the order of 0.01.

In Fig. 8 the critical values of β are plotted as function of h for $L_R = 1$, $r = 10^3$, $h = 0.01$, $\theta_0 = 0.15$. Two values of the Lewis number for fuel are used: for $L_A = 10$ the travelling instability and fold bifurcation curves are represented by the solid and the dashed lines, respectively, while for $L_A = 0.8$ the cellular instability and the fold bifurcation loci are plotted with the dotted and the dash-dotted lines, respectively. It is seen that as the heat loss parameter tends to zero the critical values β_c for fold bifurcation become large for both $L_A = 0.8$ and 10. In contrast to that the neutral stability boundaries for these two cases are presented by almost parallel curves shifted over β. The functions $\beta_c(h)$ for the onset of travelling and

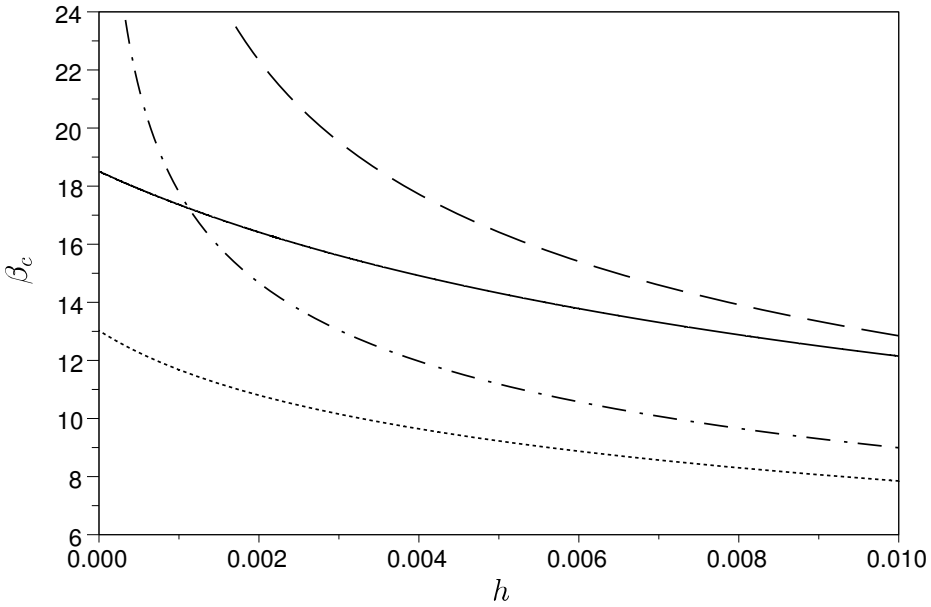

Fig. 8 The dependence of critical values of β on h for $L_R = 1$, $r = 10^3$, $h = 0.01$, $\theta_0 = 0.15$ and different values of L_A: (i) the travelling instability and fold bifurcation loci are shown with the solid and the dashed lines, respectively, for $L_A = 10$; (ii) the cellular instability and the fold bifurcation loci are plotted with the dotted and the dash-dotted lines, respectively, for $L_A = 0.8$.

cellular instabilities are characterized by finite value of $d(\ln \beta_c)/dh$ at $h = 0$, which can be estimated to be of the order of $O(10^2)$. This is two orders of magnitude larger than the corresponding derivative $d(\ln \beta_c)/dk(0)$. In other words the critical parameter values for the neutral stability boundary and fold bifurcation are less sensitive to the variation of k, than to the modification of the heat loss parameter.

3.4 Pulsating and cellular waves

As a next step we investigate the properties of two dimensional solutions which emerge as the critical parameter values for the travelling or cellular instabilities are crossed in the parameter space. The governing equations (4) are solved in a sufficiently large rectangular coordinate region with the boundary conditions similar to (6), where ξ is replaced with x, imposed at the edges of the space grid along the y axis and zero flux conditions for θ, y_A, and y_R for the edges along the x axis. The length of the region along the x direction is chosen to be sufficiently large so that the boundary conditions (6) are satisfied with reasonable accuracy. The length of the region in the y direction is chosen so as to accommodate several periods of the transverse perturbation structure which is estimated using the dispersion relations calculated from the linear stability analysis as discussed in the previous section. For our numerical algorithm we use the method of sequential splitting with respect to physical processes, a version of predictor-corrector scheme. Initially we solve the set of ordinary differential equations which describe the

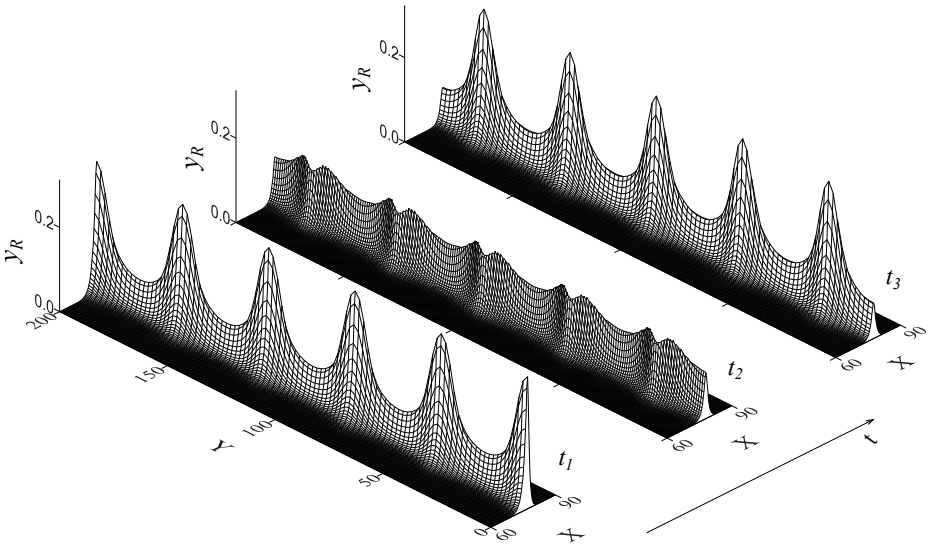

Fig. 9 The distribution of radicals y_R for pulsating wave at three moments of time $t_0 = 0.0$, $t_1 = 11$, and $t_2 = 14$ along a single period of pulsations $T = 29$ for $L_A = 10.0$, $L_R = 1.0$, $r = 1000$, $k = 0.1$, $h = 0.0$, $\beta = 14.2$.

temperature and the species concentration variations due to the branching and recombination reactions by using the fourth order Runge–Kutta algorithm. As a next step, equations of heat and mass transfer for fuel and radicals are solved by the method of alternating directions with the Crank-Nicholson scheme of the second order approximation in space and time. The initial conditions for the numerical algorithm are taken in a form of the travelling wave solution (or autowave) of (5).

As the critical parameter values for the travelling instability are crossed in the parameter space a pulsating two dimensional solution emerges. This type of solution is illustrated in Fig. 9 where the distribution of radicals y_R is shown for $L_A = 10.0$, $L_R = 1.0$, $r = 1000$, $k = 0.1$, $h = 0.0$, $\beta = 14.2$ at three moments of time $t_0 = 0.0$, $t_1 = 11$, and $t_2 = 14$ along a single period of pulsations $T = 29$. Since the solution is periodic in time, t is counted from zero to T. The pulsating wave propagates along the x axis and in Fig. 9 just a fraction of the full domain of integration over x is shown. The coordinate x here corresponds to coordinate frame moving with the average over period of time flame speed. The whole range of integration domain over y is plotted in Fig. 9 and it accommodates five full periods of the spatial structure of the solution in the transverse direction. It is seen that the pulsating solution has a from of the standing wave along the y axis. Starting from t_0 to t_3 the phase shift over π is developed i.e. the locations of peaks and deeps along y-direction completely interchange. At the intermediate point t_2 the distributions of y_R over y-axis becomes quite uniform with local minimum and maximum values of radical concentration close to each other. The pulsating combustion waves travel on average with velocities smaller than the flame speed for the travelling combustion waves for the same parameter values. For parameters listed in the Fig. 9 caption the pulsating wave speed $u = 0.4$, while the unstable travelling wave has $u = 0.45$.

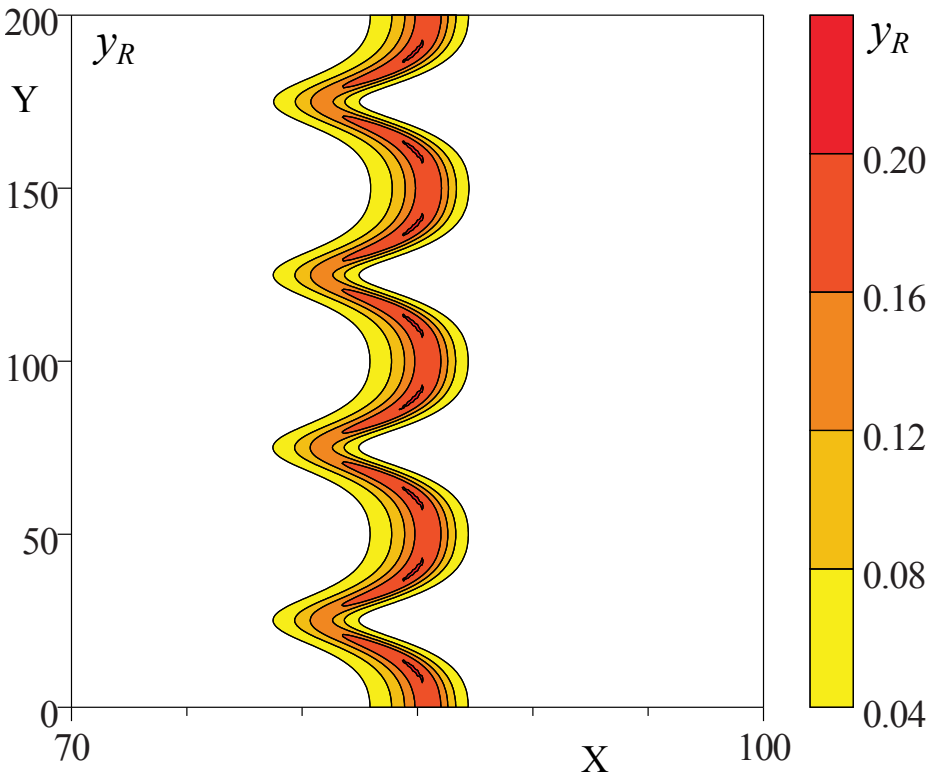

Fig. 10 The distribution of radicals y_R in cellular wave for $L_A = 0.65$, $L_R = 1.0$, $r = 1000$, $k = 0.01$, $h = 0.01$, $\beta = 8.0$.

It is important to note that the travelling instabilities and Hopf bifurcation occur for the choice of parameters as in Fig. 9 at $\beta \approx 13.8$ and $\beta \approx 14.1$, respectively. Thus the periodic solution exists in the adiabatic case beyond both critical values for the onset of one- and two-dimensional instabilities. We have found the pulsating solutions with more complex dynamical behaviour for large β as well. In the nonadiabatic case for $h = 0.001$ the pulsating solutions exist beyond the critical β for the emergence of travelling instabilities, however, they exhibit extinction before the value of β for the Hopf bifurcation is reached. For $h = 0.01$ no pulsating solutions have been found and the flame quenching is observed as the neutral stability is crossed.

Crossing the neutral stability boundary for the case of $L_A < 1$ results in the formation of cellular waves, which represent two dimensional corrugated solutions steadily propagating without changing their structure and speed. An example of such travelling wave solution is illustrated in Fig. 10, where the distribution of radicals y_R in cellular wave is shown as a contour plot for $L_A = 0.65$, $L_R = 1.0$, $r = 10^3$, $k = 0.01$, $h = 0.01$, $\beta = 8.0$. Here x is the coordinate in the frame comoving with the wave, whereas y is the coordinate in the direction transverse to the propagation direction i.e. x-axis. Once again only a part of the integration range over x is shown in Fig. 10 for illustrative purposes. The whole range of x variation is a order of magnitude larger. As the bifurcation parameter e.g. L_A is modified from

the critical value for the onset of instabilities the flame front becomes corrugated, the planar front losses stability and there emerge well structured cells, which are periodic in y-direction. As a result of such bifurcation the flame surface increases, which is accompanied by the growth of the propagation velocity in comparison to the planar regime of deflagration. For the choice of parameters shown in the caption to Fig. 10 the critical value of the Lewis number for fuel is about 0.81 and so at $L_A = 0.65$ the corrugated structure of the combustion wave is well developed in the form of the alternating crests and concaves. Exactly four cells are fitted in the range of y coordinate variation from 0 to 200. The cellular wave propagates with $u \approx 0.56$, which is higher than the velocity of planar deflagration for the same parameter values, $u \approx 0.52$, as a results of flame front corrugation.

4 Conclusions

In this paper we numerically study the effect of depletion of the radical concentration on the properties and stability of freely propagating flames with chain-branching reaction mechanism. We mainly focus on the qualitative analysis and the well known Zeldovich–Barenblatt model is taken to describe the chain-branching combustion chemistry. It is supplemented by additional stage of direct first order reaction of conversion of radicals into the products, which is aimed to mimic in very general manner various mechanisms of depletion of the radical pool e.g. Soret diffusion, radical recombination on the reactor surface, addition of flame inhibitors etc. This additional radical sink reaction is competitive step to the recombination reaction of the main chain-branching scheme of the Zeldovich–Barenblatt model. The heat loss to the surroundings is also included in the model to make a comparison of two different quenching mechanisms possible.

It is shown that the properties of the planar deflagration waves directly depend on the rate of the radical sink reaction, k, which is scaled by characteristic rate of the recombination reaction and considered here as a small parameter. The maximum values of the flame temperature and concentration of radicals as well as the burning velocity are found to be linearly correlated with k for $k \ll 1$. The derivative of these quantities with respect to k can be estimated by the order of magnitude to be of the order of $O(1)$. Thus in order to change the concentration of radicals in the reaction zone by the order of 1% the radical sink reaction should have the rate of the same order of magnitude in comparison with the rate of the main recombination reaction. Similar estimates hold for flame temperature and normal flame speed.

Two types of critical phenomena related to the deflagration waves can be observed in the system: the loss of stability and the fold bifurcation. The former is caused by the onset of travelling or cellular instabilities. The latter is usually considered as classical quenching limit for flame propagation [34] and is defined as the turning point in the dependence of the burning velocity on parameters separating the upper and lower solution branches. The occurrence of various critical events is governed by the Lewis number for fuel, L_A. The travelling instabilities are found for Lewis numbers for fuel greater than some critical value $L_A^{BT} > 1$ associated with Bogdanov–Takens bifurcation of co-dimension two at which the neutral stability boundary and fold bifurcation loci intersect in the space of parameters. For $1 < L_A < L_A^{BT}$ the travelling wave solution (the upper branch) is completely sta-

ble up to the fold bifurcation. It should be noted that the lower solution branch is always unstable. In the case of $L_A < 1$ the cellular instabilities emerge. The neutral stability boundary and the fold bifurcation loci are found in the plane of parameters: Lewis number for fuel vs activation energy of the branching reaction. The influence of the radical sink reaction rate is manifested as the uniform shift of all critical parameters to smaller values of the activation energy with the increase of k. The relative magnitude of this modification is directly proportional to the rate of the radical sink reaction so that to obtain the reduction in any of critical parameter values of the order of 1% the reaction rate k should be of the order of 0.01. It is interesting to note that critical parameter values for the neutral stability boundary and fold bifurcation are less sensitive to the variation of k, than to the changes of the heat loss parameter, h.

The solutions emerging as the neutral stability boundary is crossed in the space of parameters are investigated. It is found that the pulsating or cellular combustion waves can be obtained for $L_A > 1$ or $L_A < 1$, respectively. Pulsating waves are two-dimensional dynamical patterns with the structure of standing wave in the transverse direction and periodic time dependence. They propagate with velocities smaller than the burning velocity of the planar deflagration. As the bifurcation parameter is increased away from the stability boundary for the travelling wave solutions the dynamics of pulsations become more complex and at certain stage the flame quenching is observed. The cellular waves appear as steadily propagating corrugated fronts with crests and concaves forming the stationary periodic structure in the transverse to flame propagation direction. The flame curvature intensifies the combustion rate and the velocity of cellular waves is larger then the burning velocity for the same parameter values. The complex temporal dynamics of cellular structures emerge as the bifurcation parameter is increased, which eventually lead to flame quenching. The scenarios of dynamical flame quenching as well as the flammability limits will be investigated in the future work.

5 Acknowledgments

This work was supported by The Ministry of Education and Science of Russian Federation (grant 14.Y26.31.0003); Far Eastern Federal University; Russian Foundation for Basic Research Grant 13-03-00282; Collaborative Research Project, Institute of Fluid Science, Tohoku University J15074. VVG is thankful to Z. Chen for fruitful discussions.

References

1. Zeldovich, Y.B., Barenblatt, G.I., Librovich, V.B., Makhviladze, G.M., *The mathematical theory of combustion and explosions* (Consultants Bureau, New York, 1985).
2. Ern, A., Giovangigli, V., Impact of detailed multicomponent transport on planar and counterflow hydrogen/air and methane/air flames. Combustion Science and Technology **149**, 157–181 (1999)
3. Yang, F., Law, C., Sung, C., Zhang, H., A mechanistic study of Soret diffusion in hydrogenair flames. Combustion and Flame **157**, 192–200 (2010)
4. Liang, W., Chen, Z., Yang, F., Zhang, H., Effects of Soret diffusion on the laminar flame speed and Markstein length of syngas/air mixtures. Proceedings of the Combustion Institute **34**, 695–702 (2013)

5. Sánchez, A.L., Williams, F.A., Recent advances in understanding of flammability characteristics of hydrogen. Progress in Energy and Combustion Science **41**, 1 – 55 (2014)
6. Han, W., Chen, Z., Effects of Soret diffusion on spherical flame initiation and propagation. International Journal of Heat and Mass Transfer **82**, 309–315 (2015)
7. Liu, J., Zhang, X., Wang, T., Hou, X., Zhang, J., Zheng, S., Numerical study of the chemical, thermal and diffusion effects of H_2 and CO addition on the laminar flame speeds of methane-air mixture. International Journal of Hydrogen Energy **40**, 8475–8483 (2015)
8. Jimenez, C., Fernández-Galisteo, D., Kurdyumov, V.N., DNS study of the propagation and flashback conditions of lean hydrogen-air flames in narrow channels: symmetric and non-symmetric solutions. Combustion and Flame (in press) (2015)
9. Vlachos, D.G., Schmidt, L.D., Aris, R., Ignition and extinction of flames near surfaces: Combustion of H_2 in air. Combustion and Flame **95**, 313–335 (1993)
10. Vlachos, D., The interplay of transport, kinetics, and thermal interactions in the stability of premixed hydrogen/air flames near surfaces. Combustion and Flame **103**, 59–75 (1995)
11. Aghalayam, P., Bui, P., Vlachos, D., The role of radical wall quenching in flame stability and wall heat flux: hydrogen-air mixtures. Combustion Theory and Modelling **2**, 515–530 (1998)
12. Aghalayam, P., Vlachos, D., Roles of thermal and radical quenching in emissions of wall-stabilized hydrogen flames. AIChE journal **44**, 2025–2034 (1998)
13. Raimondeau, S., Norton, D., Vlachos, D., Masel, R., Modeling of high-temperature microburners. Proceedings of the Combustion Institute **29**, 901–907 (2002)
14. Bai, B., Chen, Z., Zhang, H., Chen, S., Flame propagation in a tube with wall quenching of radicals. Combustion and Flame **160**, 2810 – 2819 (2013)
15. Miesse, C.M., Masel, R.I., Jensen, C.D., Shannon, M.A., Short, M., Submillimeter-scale combustion. AIChE Journal **50**, 3206–3214 (2004)
16. Saiki, Y., Suzuki, Y., Effect of wall surface reaction on a methane-air premixed flame in narrow channels with different wall materials. Proceedings of the Combustion Institute **34**, 3395 – 3402 (2013)
17. Kizaki, Y., Nakamura, H., Tezuka, T., Hasegawa, S., Maruta, K., Effect of radical quenching on CH4/air flames in a micro flow reactor with a controlled temperature profile. Proceedings of the Combustion Institute **35**, 3389 – 3396 (2015)
18. Lazarovici, A., Kalliadasis, S., Merkin, J., Scott, S., Simon, P., The propagation and inhibition of an exothermic branched-chain flame with an endothermic reaction and radical scavenging. Journal of Engineering Mathematics **49**, 41–55 (2004)
19. Simon, P.L., Scott, S.K., Kalliadasis, S., Merkin, J.H., The effect of a radical scavenger on the propagation of flames in an exothermic-endothermic system. Journal of Mathematical Chemistry **38**, 203–231 (2005)
20. Zeldovich, Y.B., Chain reactions in hot flames - an approximate theory of flame velocity. Kinetika i kataliz **2**, 305–318 (1961)
21. Liñán, A., A theoretical analysis of premixed flame propagation with an isothermal chain reaction. Tech. Rep. 1, Instituto Nacional de Tecnica Aeroespacial Madrid (Spain) (1971)
22. Gann, R.G., Guidance for advanced fire suppression in aircraft. Fire Technology **44**, 263–282 (2008)
23. Day, M., Stamp, D., Thompson, K., Dixon-Lewis, G., Inhibition of hydrogen-air and hydrogen-nitrous oxide flames by halogen compounds. Symposium (International) on Combustion, **13**, 705–712 (1971)
24. Westbrook, C.K., Numerical modeling of flame inhibition by CF_3Br. Combustion Science and Technology **34**, 201–225 (1983)
25. Babushok, V., Noto, T., Burgess, D., Hamins, A., Tsang, W., Influence of CF_3I, CF_3Br, and CF_3H on the high-temperature combustion of methane. Combustion and Flame **107**, 351–367 (1996)
26. Zeldovich, Y.B., Barenblatt, G.I., Theory of flame propagation. Combustion and Flame **3**, 61–74 (1959)
27. Dold, J.W., Weber, R.O., Thatcher, R.W., Shah, A.A., Flame balls with thermally sensitive intermediate kinetics. Combustion Theory and Modelling **7**, 175–203 (2003)
28. Sharpe, G.J., Thermal-diffusive instability of premixed flames for a simple chain-branching chemistry model with finite activation energy. SIAM Journal on Applied Mathematics **70**, 866–884 (2009)
29. Gubernov, V.V., Kolobov, A.V., Polezhaev, A.A., Sidhu, H.S., Mercer, G.N., Oscillatory thermal-diffusive instability of combustion waves in a model with chain-branching reaction and heat loss. Combustion Theory and Modelling **15**, 385–407 (2011)

30. Zhang, H., Chen, Z., Spherical flame initiation and propagation with thermally sensitive intermediate kinetics. Combustion and Flame **158**, 1520–1531 (2011)
31. Kurdyumov, V.N., Fernández-Galisteo, D., Asymptotic structure of premixed flames for a simple chain-branching chemistry model with finite activation energy near the flammability limit. Combustion and Flame **159**, 3110–3118 (2012)
32. Popp, P., Smooke, M., Baum, M., Heterogeneous/homogeneous reaction and transport coupling during flame-wall interaction. Symposium (International) on Combustion **26**, 2693–2700 (1996)
33. Gubernov, V., Kolobov, A., Polezhaev, A., Sidhu, H., Mercer, G., Period doubling and chaotic transient in a model of chain-branching combustion wave propagation. Proc. R. Soc. Lond. A **466**(2121), 2747–2769 (2010)
34. Spalding, D.B., A theory of inflammability limits and flame-quenching. Proceedings of the Royal Society A: Mathematical, Physical and Engineering Sciences **240**, 83–100 (1957)